

The Power Law of Sensory Adaptation: Simulation by a Model of Excitability in Spider Mechanoreceptor Neurons

ANDREW S. FRENCH and PÄIVI H. TORKKELI

Department of Physiology and Biophysics, Dalhousie University, Halifax, NS, Canada, B3H 1X5

(Received 1 May 2007; accepted 9 October 2007; published online 19 October 2007)

Abstract—The power law of sensory adaptation was introduced more than 50 years ago. It is characterized by action potential adaptation that follows fractional powers of time or frequency, rather than exponential decays and corresponding frequency responses. Power law adaptation describes the responses of a range of vertebrate and invertebrate sensory receptors to deterministic stimuli, such as steps or sinusoids, and to random (white noise) stimulation. Hypotheses about the physical basis of power law adaptation have existed since its discovery. Its cause remains enigmatic, but the site of power law adaptation has been located in the conversion of receptor potentials into action potentials in some preparations. Here, we used pseudorandom noise stimulation and direct spectral estimation to show that simulations containing only two voltage activated currents can reproduce the power law adaptation in two types of spider mechanoreceptors. Identical simulations were previously used to explain the different responses of these two types of sensory neurons to step inputs. We conclude that power law adaptation results during action potential encoding by nonlinear combination of a small number of activation and inactivation processes with different exponential time constants.

Keywords—Action potential, Neural coding, Information capacity, Ion channel, Hodgkin–Huxley, Frequency response.

INTRODUCTION

In a seminal study, Landgren²² examined the detailed static and dynamic properties of action potential firing in cat carotid baroreceptor neurons as a function of blood pressure. He found that a step increase in blood pressure increased the rate of firing, but the firing then decreased, or adapted to the step. The decrease in rate of firing versus time, $g(t)$, was not exponential, but instead followed a power law equation:

$$g(t) = at^{-k} \quad (1)$$

where t is time after the step, a and k are constants. The constant k , which is now called the fractional exponent, was 0.65 in one example, but varied depending on the step amplitude.

Following this, Chapman and Smith⁶ re-examined the adapting response of an insect mechanoreceptor, the cockroach tactile spine. They pointed out that power law behavior would lead to a frequency response function of the form:

$$G(f) = Af^k \quad (2)$$

where $G(f)$ is gain as a function of frequency, f , A is a constant and k is the same fractional exponent. The phase relationship, $P(f)$, of the same system would be:

$$P(f) = k \cdot 90^\circ \quad (3)$$

so that the output signal would lead the input in phase, independent of frequency for $k > 0$. Adaptation of firing in the cockroach tactile spine was found to fit the power law equations with both step and sinusoidal stimuli.⁶

A later review of power law adaptation in sensory receptors concluded that the behavior was widespread, with further examples in crayfish stretch receptors, *Limulus* eye, mammalian muscle spindles and spider slit sensilla.^{1,3,5,32} Subsequently, power law adaptation has been shown for mechanical stimulation of frog skin mechanoreceptors,³⁷ cat skin mechanoreceptors,²⁴ monkey skin touch receptors²⁵ and different groups of spider slit sensilla.^{4,13} In each case the estimated fractional exponent, k , was between zero and unity.

What causes power law adaptation? Chapman and Smith⁶ listed processes that could contribute. These included the viscoelastic properties of mechanical coupling to the receptor neuron, dynamic properties of the mechanotransduction channels, action potential encoding, and unspecified nonlinear mechanisms at any stage. Brown and Stein⁵ developed a specific

Address correspondence to Andrew S. French, Department of Physiology and Biophysics, Dalhousie University, Halifax, NS, Canada, B3H 1X5. Electronic mail: andrew.french@dal.ca

mechanical model of power law adaptation in crayfish stretch receptors, but they also suggested that the power law could arise from a combination of multiple exponential relaxation processes occurring at each stage between mechanical input and action potential output. They also noted that the power law is a linear function, so it is not necessary to invoke nonlinear behavior to explain it, although nonlinear contributions are not precluded. Thorson and Biederman-Thorson³² supported the idea that a combination of exponential relaxation processes with distributed time constants was responsible, although they emphasized processes occurring before action potential production.

French⁹ recorded the receptor potential before action potential encoding in the cockroach tactile spine. Surprisingly, there was no detectable adaptation in this receptor potential, even though there was power law adaptation of action potentials.^{6,12} This was followed by the complementary finding that direct electrical stimulation of action potentials, which bypassed the mechanotransduction stage, produced the familiar power law adaptation.¹⁰ Similar results were found in spider slit sensilla, where receptor current did not adapt,¹⁷ while electrical stimulation produced power law adaptation.¹³

It should also be noted that the power law phase prediction (Eq. 3) has been found whenever phase was measured in receptors with power law gain behavior, but experiments often reported additional phase lags at higher frequencies that could be explained by a time delay. One cause of such delay can be action potential conduction to the recording electrode.³⁷

The available data indicate that power law adaptation arises during action potential encoding from the receptor potential, but what components of an electrically excitable membrane are required? Voltage activated ion channels are the primary agents in the production and timing of action potentials. Ion channel kinetics can display complex dynamics, including power law distributions of event durations^{23,27} and power law relationships between activation and inactivation kinetics.³³ Distributed ion channel behavior can lead to power law firing properties,¹⁶ but are distributed properties required to explain power law adaptation?

We have previously shown that major features of action potential firing and modulation in the two types of spider VS-3 slit sensilla can be simulated by a model containing Hodgkin–Huxley style representations of the two major voltage activated ion currents: inactivating Na⁺ and delayed rectifier K⁺ currents.^{14,34} Here, we show that the same simulations can produce power law adaptation of action potential firing that agrees well with the experimental data over the measured dynamic range. We also measured coherence functions and derived information capacities from

them for each simulation. While not directly related to power law adaptation these measurements provided additional evidence that the simulations matched the experimental data, and provide indications of the inherent noise levels in the experimental neurons.

METHODS

Membrane Current Simulation

Simulation of membrane currents in spider VS-3 mechanosensory neurons was performed by methods described previously.^{14,34} The approach was based on the Hodgkin–Huxley model¹⁹ using the exponential Euler method for integrating the differential equations²⁶ with a step duration of 20 μ s. Time constants of activation, inactivation, and recovery from inactivation, τ , were represented by:

$$\tau = \tau_{\max} \frac{e^{\delta(V-V_{50})/s}}{(1 + e^{(V-V_{50})/s})}, \quad 0 < \delta < 1 \quad (4)$$

where τ_{\max} is the maximum value of τ , and δ is a constant.²⁰ This formulation simplifies simulation and allows the inclusion of a different time constant for recovery from inactivation in the model, based on experimental measurements of sodium channel inactivation in these neurons.³⁵ The value of τ_{\max} for inactivation switched between two values, depending on whether the inactivation parameter, h , was increasing or decreasing during each time step. An alternative approach⁸ is to use different values of τ_{\max} for values of h above and below 0.5. Previous simulations³⁴ showed that both methods gave similar results, but the slope method was closer to the experimental measurements used to obtain τ_{\max} .

The software was constructed as a C++ class library, similar to the Conical simulation system³¹ but restricted to a single isopotential spherical cell. All simulations were performed on IBM-compatible personal computers. Stimulating membrane currents are reported as positive for depolarization throughout.

Frequency Response Estimation

Pseudorandom Gaussian white noise was used as the input signal, followed by direct spectral estimation to obtain the frequency response and coherence functions.² Noise was generated from a 33-bit binary sequence algorithm clocked to give a simulated bandwidth of 0–300 Hz. This frequency range was chosen to match the bandwidth used in experimental measurements from spider VS-3 neurons.¹³ The bandwidth in this earlier work was limited by the intracellular stimulation electronics. Noise values were adjusted to

give the desired root mean square (RMS) current amplitude, and stimulus data points between the clocked noise values were filled in by linear interpolation. Simulations were run to generate 100 s of membrane potential data, including action potentials, (Fig. 1) and then re-sampled at 10 kHz to generate a simulated voltage recording.

Further processing of the voltage recordings proceeded identically to previous analysis of experimental recordings,¹³ using the same software. Action potentials were separated from the underlying continuous membrane potential by an algorithm that identified action potentials as a minimum increase of 20 mV, followed by a minimum decrease of 20 mV, all within less than 2 ms. Separations were inspected visually, together with the original recording, to ensure that the algorithm functioned properly. Separated action potentials were stored as times of occurrence, while the gap caused by action potential separation was filled by linear interpolation between its ends. Each action potential was convolved with a $\sin(x)/x$ function and then re-sampled at regular 1 ms intervals to band-limit the signal to the range 0–500 Hz.¹¹ Membrane potential signals were digitally re-sampled by averaging to give a 1 ms sample interval.

Sampled signals were transformed to the frequency domain using the fast Fourier transform⁷ using

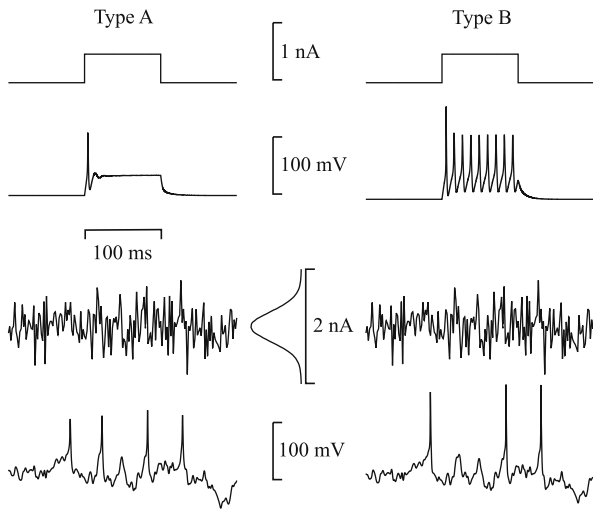


FIGURE 1. Simulated sensory neuron responses to step and random noise stimuli. Current traces and resulting voltage responses are shown during current-clamp stimulation. Depolarizing steps of 0.5 nA to Type A (left) and Type B (right) neurons produced a single action potential and a burst of action potentials, respectively (upper panels). Randomly fluctuating current stimulation with amplitude 0.25 nA RMS produced fluctuating membrane potentials with superimposed action potentials in both neuron types (lower panels). The randomly fluctuating current had a bandwidth of 0–300 Hz and was approximately Gaussian distributed. A normalized histogram of the current amplitude distribution obtained from 100 s of stimulation is shown between the two random current traces.

segments of 1024 input–output data pairs. Frequency response functions (gain and phase) between the input (mechanical displacement or membrane potential) and the output (action potentials) were calculated and plotted as Bode plots of phase and log gain versus log frequency.

A linear relationship was fitted to the log gain versus log frequency data by linear regression, corresponding to the power law model (Eq. 2). The fractional exponent, k , was used to predict the phase relationship (Eq. 3). Residual phase lag, $P_r(f)$, after subtracting the power law phase shift, was modeled by a fixed time delay, Δt , and was fitted by linear regression between residual phase and linear frequency:

$$P_r(f) = -\Delta t f 360^\circ \quad (5)$$

The coherence function, $\gamma^2(f)$, was calculated from the same data and plotted together with the frequency response functions. Coherence is a normalized correlation function that measures the proportion of the output signal that can be accounted for by linear transformation of the input signal.² Its value is unity for a linear, noise-free system and is reduced by the presence of nonlinearity or uncorrelated noise in the system. The information capacity, R , for each recording was calculated from the coherence function:^{21,30}

$$R = \int \log_2\{1/(1 - \gamma^2(f))\} df \quad (6)$$

For each simulated condition, ten equal length segments were created and each segment was processed to give the fitted parameters A , k , Δt , and R . Mean values and standard deviations were reported from each set of 10 parameter values.

RESULTS

Each of the two types of spider VS-3 neuron was simulated as a spherical cell containing a single sodium current with voltage dependent activation and inactivation, plus a single potassium current with voltage dependent activation (delayed rectifier). These models and their parameters (Table 1) were based on those used previously to simulate spider VS-3 neurons.³⁴ The models each included separate time constants for the development and recovery from inactivation, switching between the two time constants as inactivation increased or decreased. This approach was based on experimental measurements of sodium current in these neurons,³⁵ which necessarily estimated development and recovery from inactivation as completely separate processes, and has proved successful in modeling several aspects of firing behavior in these neurons.^{14,34}

TABLE 1. Parameters used during simulation of Type A and Type B neurons are identified by conventional symbols,¹⁹ except for δ (Eq. 4).

	Type A		Type B	
<i>Passive parameters</i>				
Diameter (μm)	54		54	
Specific resistance (Ωm^2)	1.68		1.68	
Specific capacitance (F/m^2)	0.01		0.01	
<i>Voltage-activated currents (activation)</i>				
	K⁺	Na⁺	K⁺	Na⁺
G_{max} (nS)	200	400	200	400
V_{rev} (mV)	-85.1	99.0	-85.1	99.0
Exponent of m, n	4	3	4	3
V_{50} (mV)	-50	-45	-50	-45
s (mV)	10	5	10	5
τ_{max} (ms)	5	1	6	1
δ	0.4	0.4	0.4	0.4
<i>Voltage-activated currents (inactivation)</i>				
Exponent of h		1		1
V_{50} (mV)		-60		-60
s (mV)		5		9
τ_{max} (ms)		20		20
δ		0.4		0.4
τ_{recovery} (ms)		120		40

τ_{max} and τ_{recovery} refer to time constants of inactivation and recovery from inactivation respectively.

A similar approach was used by others in simulating voltage-activated calcium channels.⁸ The major differences between the currents in Type A and Type B neurons, and their simulations, are in the rate of sodium inactivation, which is faster in Type A neurons, and the rate of recovery from inactivation, which is faster in Type B neurons.^{34,35}

Simulated Voltage Responses

Simulated responses to depolarizing current steps in Type A and Type B neurons (Fig. 1) have been described previously.³⁴ Type A neurons typically have

a threshold for current injection of 0.1–0.5 nA and fire only one or two action potentials regardless of step amplitude. Type B neurons have a similar threshold but produce bursts of repetitive firing that can last for more than 100 ms, in strong contrast to Type A neurons. When the two neuron types are stimulated with randomly fluctuating membrane current there are resulting fluctuations in membrane potential that lead to action potentials if the stimulation is strong enough. Both neuron types produce action potentials continuously for long periods with random stimulation. This has been shown in real neurons¹³ and was also found in the present simulations, so the randomly varying

membrane potential and resultant action potentials (Fig. 1) would continue indefinitely.

Frequency Response Functions

Action potentials were separated from the underlying membrane potential fluctuations (Methods) and frequency response functions calculated between membrane potential, as the input to the neuronal encoder, and the action potentials as output. Frequency responses showed the typical power law relationship (Eqs. 2 and 3) in both the gain and the phase at low frequency (Fig. 2). Additional phase lag with increasing frequency was well fitted by a simple time delay (Eq. 5).

Power Law Parameters

Previous measurement from spider VS-3 neurons explored the fitted power law parameters as a function of action potential firing rate, with varying amplitudes of noise stimulation.¹³ However, intracellular recordings usually cause additional leakage current that depolarizes neurons, and some of the variation in firing

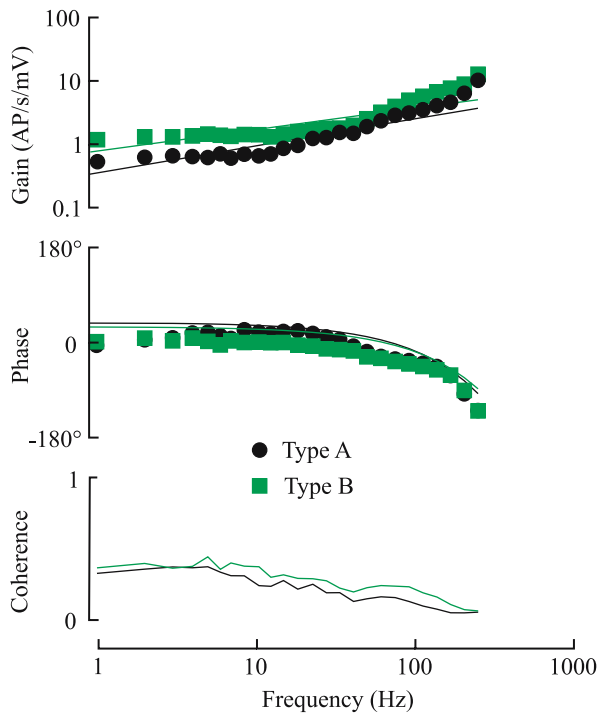


FIGURE 2. Frequency response and coherence functions between membrane potential (input) and action potentials (output) obtained from simulated Type A and Type B neurons during random current stimulation. Filled symbols are simulated data from Type A (circles) and Type B (squares). Solid lines show the fitted parameters of Eqs. (2), (3), and (5) with $k = 0.43$, $\Delta t = 1.51$ ms (Type A) and $k = 0.34$, $\Delta t = 1.32$ ms (Type B). Information capacity from Eq. (6) was 79.4 Bits/s (Type A) and 124.9 Bits/s (Type B).

rate was probably caused by leakage current. Therefore, we used a range of noise stimulus amplitudes (0.25–1.25 nA RMS in steps of 0.25 nA RMS) and two levels of depolarizing leakage current (50 and 100 pA) to generate a range of action potential firing (2.4–42.5 AP/s) that approximated the range found in the original experiments. Figures 3–6 show average parameter values from 10 simulations at each different firing rate plotted on the same axes as the previously published experimental data.¹³

Mean values for the power law exponent, k , and time delay, Δt , were closely comparable to the experimental values¹³ for both neuron types (Table 2 and horizontal lines in Figs. 3 and 4). Plots of k versus firing rate (Fig. 3) were similar, both in the mean values and in the tendency for higher values at lower firing rates. Simulated Type A neurons had a higher mean value of k , corresponding to more rapid adaptation, as also seen in experimental measurements. Plots of simulated Δt versus firing rate were also closely similar to experimental values (Fig. 4). Simulated and experimental Type A neurons had higher mean values of Δt than Type B neurons.

Simulated information capacity measurements were converted to information per action potential

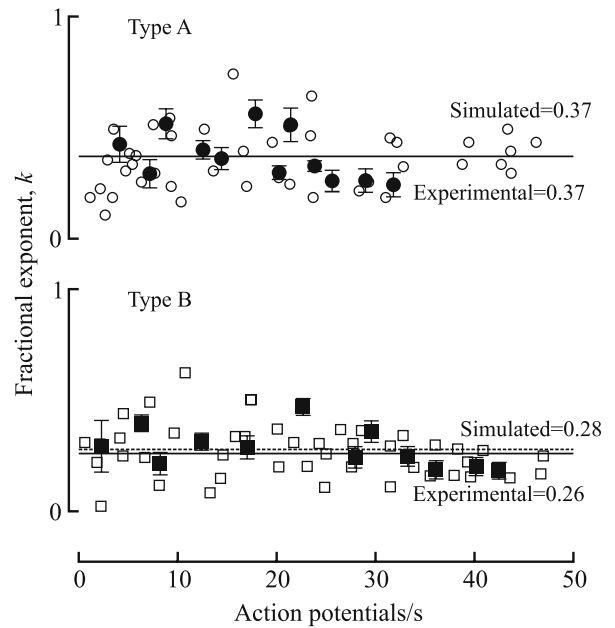


FIGURE 3. Fitted fractional exponent, k , of simulated neurons versus their action potential firing rates. Filled circles show fitted values of k for Type A and filled squares for Type B neurons (mean and standard deviation from 10 simulations). Smaller unfilled symbols show the original experimental data from real neurons published previously.¹³ Dashed lines (Simulated) show mean values of k from Table 2. Solid lines (Experimental) show the corresponding mean values obtained from the real neurons.¹³

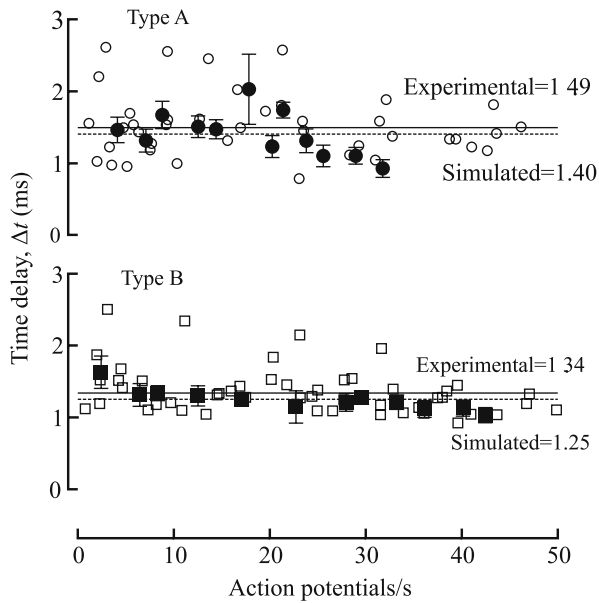


FIGURE 4. Fitted Time delay, Δt , of simulated neurons versus their action potential firing rates. Filled circles show fitted values of Δt for Type A and filled squares for Type B neurons (mean and standard deviation from 10 simulations). Smaller unfilled symbols show the original experimental data from real neurons published previously.¹³ Dashed lines (Simulated) show mean values of Δt from Table 2. Solid lines (Experimental) show the corresponding mean values obtained from the real neurons.¹³

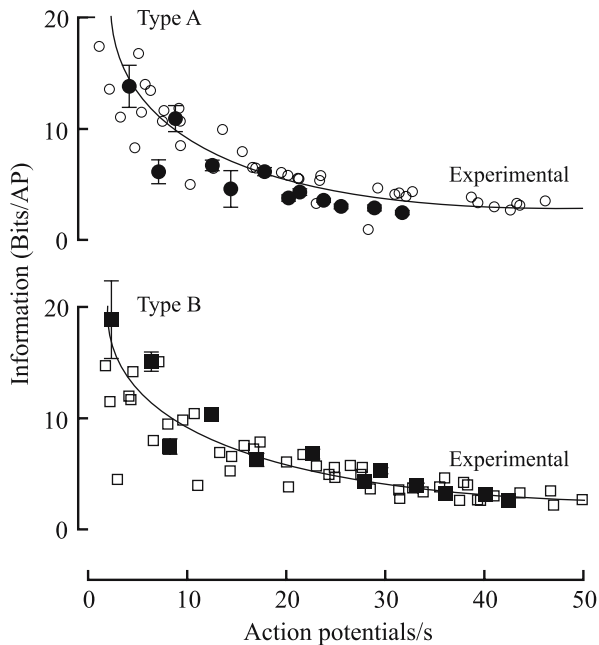


FIGURE 5. Information per action potential versus action potential firing rate for simulated Type A (filled circles) and Type B (filled squares) neurons (mean and standard deviation from 10 simulations). Smaller unfilled symbols show the original experimental data from real neurons published previously.¹³ The values were calculated by dividing information capacity (Bits/s) by firing rate (AP/s). Solid lines (Experimental) show previously published lines that were drawn by eye through measurements made on the real neurons.¹³

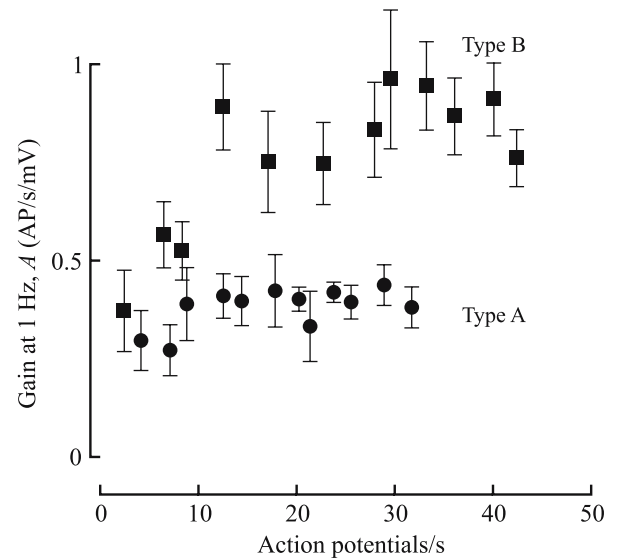


FIGURE 6. Gain at 1 Hz, A , versus firing rate for simulated Type A (circles) and Type B (squares) neurons (mean and standard deviation from 10 simulations). No experimental data is available for comparison.

(Fig. 5). Information per action potential approached 20 Bits/AP at low firing rates but decreased with firing rate to asymptotic values of ~ 3 Bits/AP. These data were closely similar to the experimental measurements.¹³ Mean values of information capacity were higher in simulated Type B neurons than in Type A neurons (Table 2). This difference was not seen in the experimental data.

Parameter A , the gain at 1 Hz, increased with firing rate in the simulated neurons and was significantly higher in Type B neurons (Fig. 6, Table 2). This parameter is difficult to interpret in terms of general neuronal properties. While it reflects the neuronal sensitivity, or excitability, at 1 Hz, the sensitivity at other frequencies depends on the combination of both A and k . Experimental values of A have not been reported previously.

TABLE 2. Comparison of power law frequency response parameters and information capacities obtained from simulated and experimental measurements in spider VS-3 neurons.

	Type A		Type B	
	Simulated	Experimental	Simulated	Experimental
k	0.37 ± 0.11	0.37 ± 0.14	0.28 ± 0.09	0.26 ± 0.11
Δt (ms)	1.40 ± 0.30	1.49 ± 0.43	1.25 ± 0.15	1.34 ± 0.31
R (bits/s)	79 ± 17.3	118 ± 29.8	113 ± 32.9	118 ± 27.7
A (AP/s/mV)	0.37 ± 0.10		0.76 ± 0.18	
n	12	26	12	37

All experimental data are taken from Table 1 of Ref. 14.

DISCUSSION

Power Law Sensory Adaptation

Simulated VS-3 neurons not only gave frequency response functions that could be fitted by the power law (Eqs. 2 and 3), but the parameters obtained were closely similar to those obtained from experimental measurements on real neurons over a range of action potential firing rates (Table 2 and Figs. 3–5). This supports the hypothesis that the physical basis of power law behavior in these sensory neurons is a combination of several different exponential processes in their action potential encoding membranes.¹⁵ The present simulations contained four different time constants (Na⁺ and K⁺ activation, Na⁺ inactivation and recovery from inactivation) distributed over the range of 1–120 ms (Table 1). Real VS-3 neurons contain several additional currents^{28,29} that could contribute other exponential components, although they are clearly not required to explain the major features of action potential activity produced by step or noise currents.

Time Delay

Action potentials in VS-3 neurons have duration of ~2 ms, so there is an inherent time delay of ~1 ms between action potential initiation and detection of the peak depolarization. The observed delays of < 1.5 ms can probably be entirely explained by the time required to activate the Na⁺ channels, which have an activation time constant of 1 ms, and reach the peak depolarization. It was previously observed that mechanically stimulated action potentials are produced with significantly less time delay (< 1.0 ms).¹³ Other evidence supports the existence of a distally located mechanotransduction site with lower threshold and greater excitability than the cell soma,^{17,18} which could explain the reduced delay.

Differences between Type A and Type B Neurons

In contrast to the strong difference in firing behavior seen with step depolarizations, there were more subtle differences between their responses to noise stimulation for both experimental¹³ and simulated data (Table 2). Type A neurons had larger mean values of the power law exponent, k , corresponding to faster adaptation, as seen in the step response, and a longer time delay, Δt , which could reflect the lower excitability seen in the step response.

Simulated Type B neurons had a higher mean information capacity that was not seen in experimental neurons¹³ and is difficult to interpret here because simulated Type A neurons did not achieve such

high firing rates as Type B neurons (Fig. 5). Simulated Type B neurons also had higher values of the gain at 1 Hz, parameter A (Table 2, Fig. 6), again reflecting their ability to fire more action potentials, especially at low frequencies. The step response (Fig. 1) is an extreme illustration of this difference, with Type B neurons continuing to fire with constant (0 Hz) depolarization.

This difference in adaptation behavior of the two neuron types seems to be dominated by the differences in sodium channel inactivation, as shown previously.³⁴ In terms of power law parameters, this leads to stronger low frequency response and a higher value of parameter A for Type B neurons, but more sensitivity to higher frequencies and a higher value of parameter k for Type A neurons.

Information Capacity

Information capacity divided by firing rate reached asymptotic values of ~3 Bits/AP. This is comparable to the values obtained in experimental VS-3 neurons.¹³ Similar values were obtained for mechanotransduction in cricket hair receptors.³⁶ Combined with maximum firing rates of about 50 action potentials/s, these values imply a maximum information capacity of ~150 Bits/s, which is comparable to the maximum values of ~200 Bits/s found in these and other spiking neurons, whereas the information capacities of non-spiking neurons can exceed 2000 Bits/s.²¹ The estimation of information capacity used here (Eq. 6) was based on the coherence function. Since the data were obtained by simulation there was no uncorrelated noise, and the reduction in coherence below unity reflects nonlinear properties of the simulated currents. Again, it is difficult to compare the mean information capacities between simulated and experimental neurons because the parameter varies with firing rate and we were unable to exactly reproduce the collection of firing rates observed experimentally. However, the similar asymptotic values suggest that real VS-3 neurons have little inherent membrane noise.

In the simulations here, and in the experimental work on real neurons,¹³ we used membrane potential as the input and action potentials as the output. The experimental work also gave power law relationships between mechanical stimulation and action potentials. Conversion of mechanical stimuli to membrane current, and hence membrane potential and action potentials, occurs near the distal tips of sensory dendrites in these neurons.^{17,18} The detailed biophysical properties of the mechanotransduction mechanisms are not well understood, but the evidence suggests that relatively short time constants are involved, which would account for the similar dynamic response to

mechanical displacement or membrane potential. Any addition of inherent noise to action potential encoding probably occurs at this distal location.

CONCLUSIONS

More than 50 years after Landgren²² described power law adaptation in mammalian baroreceptors, we conclude that this form of sensory adaptation can be produced by neural action potential encoders as they combine nonlinear voltage activated membrane currents with several different time constants of activation and inactivation. The dynamic range of the power law behavior in this case was limited by experimental conditions to about two log units, and cannot be assumed to apply over a much wider range. In addition, other linear or nonlinear mechanisms, such as viscoelastic mechanical components, channels transducing external stimuli, or more distributed ion channel properties may make additional contributions to sensory receptor adaptation, and may even help to extend the power law behavior over a wider time or frequency range. Nevertheless, we conclude that the primary components producing power law behavior in these sensory neurons are conventional voltage activated Na⁺ and K⁺ channels.

ACKNOWLEDGMENT

Supported by grants from the Canadian Institutes of Health Research.

REFERENCES

- ¹Barth, F. G. Ein einzelnes Spaltsinnesorgan auf dem Spinnentarsus: seine Erregung in Abhängigkeit von den Parametern des Luftschallreizes. *Z. Vergl. Physiol.* 55: 407–449, 1971.
- ²Bendat, J. S., and A. G. Piersol. *Engineering Applications of Correlation, Spectral Analysis*. New York: John Wiley & Sons, pp. 1–302, 1980.
- ³Biederman-Thorson, M., and J. Thorson. Dynamics of excitation and inhibition in the light-adapted Limulus Eye *in situ*. *J. Gen. Physiol.* 58:1–19, 1971.
- ⁴Bohnenberger, J. Matched transfer characteristics of single units in a compound slit sense organ. *J. Comp. Physiol.* 142:391–402, 1981.
- ⁵Brown, M. C., and R. B. Stein. Quantitative studies on the slowly adapting stretch receptor of the crayfish. *Kybernetik* 3:175–185, 1966.
- ⁶Chapman, K. M., and R. S. Smith. A linear transfer function underlying impulse frequency modulation in a cockroach mechanoreceptor. *Nature* 197:699–700, 1963.
- ⁷Cooley, J. W., and J. W. Tukey. An algorithm for the machine calculation of complex Fourier series. *Math. Comput.* 19:297–301, 1965.
- ⁸Destexhe, A., and J. R. Huguenard. Nonlinear thermodynamic models of voltage-dependent currents. *J. Comput. Neurosci.* 9:259–270, 2000.
- ⁹French, A. S. Dynamic properties of the action potential encoder in an insect mechanosensory neuron. *Biophys. J.* 46:285–289, 1984.
- ¹⁰French, A. S. The receptor potential and adaptation in the cockroach tactile spine. *J. Neurosci.* 4:2063–2068, 1984.
- ¹¹French, A. S., and A. V. Holden. Alias-free sampling of neuronal spike trains. *Kybernetik* 8:165–171, 1971.
- ¹²French, A. S., A. V. Holden, and R. B. Stein. The estimation of the frequency response function of a mechanoreceptor. *Kybernetik* 11:15–23, 1972.
- ¹³French, A. S., U. Höger, S. Sekizawa, and P. H. Torkkeli. Frequency response functions and information capacities of paired spider mechanoreceptor neurons. *Biol. Cybern.* 85:293–300, 2001.
- ¹⁴French, A. S., I. Panek, and P. H. Torkkeli. Shunting versus inactivation: simulation of GABAergic inhibition in spider mechanoreceptors suggests that either is sufficient. *Neurosci. Res.* 55:189–196, 2006.
- ¹⁵French, A. S., and P. H. Torkkeli. The time course of sensory adaptation in the cockroach tactile spine. *Neurosci. Lett.* 178:147–150, 1994.
- ¹⁶Gilboa, G., R. Chen, and N. Brenner. History-dependent multiple-time-scale dynamics in a single-neuron model. *J. Neurosci.* 25:6479–6489, 2005.
- ¹⁷Gingl, E., and A. S. French. Active signal conduction through the sensory dendrite of a spider mechanoreceptor neuron. *J. Neurosci.* 23:6096–6101, 2003.
- ¹⁸Gingl, E., A. S. French, I. Panek, S. Meisner, and P. H. Torkkeli. Dendritic excitability and localization of GABA-mediated inhibition in spider mechanoreceptor neurons. *Eur. J. Neurosci.* 20:59–65, 2004.
- ¹⁹Hodgkin, A. L., and A. F. Huxley. A quantitative description of membrane current and its application to conduction and excitation in nerve. *J. Physiol.* 117:500–544, 1952.
- ²⁰Johnston, D., and S. M. S. Wu. *Foundations of Cellular Neurophysiology*. Cambridge, MA: MIT Press, pp. 1–676, 1995.
- ²¹Juusola, M., and A. S. French. The efficiency of sensory information coding by mechanoreceptor neurons. *Neuron* 18:959–968, 1997.
- ²²Landgren, S. On the excitation mechanism of the carotid baroreceptors. *Acta Physiol. Scand.* 26:1–34, 1952.
- ²³Liebovitch, L. S., J. Fischbarg, and J. P. Koniarek. Ion channel kinetics: a model based on fractal scaling rather than multistate markov processes. *Math. Biosci.* 84:37–68, 1987.
- ²⁴Looft, F. J. Linear systems analysis of cutaneous type I mechanoreceptors. *IEEE Trans. Biomed. Eng.* 37:565–573, 1990.
- ²⁵Looft, F. J. Response of monkey glabrous skin mechanoreceptors to random-noise sequences: III. spectral analysis. *Somatosens. Mot. Res.* 13:235–244, 1996.
- ²⁶MacGregor, R. J. *Neural and Brain Modeling*. San Diego, CA: Academic Press, pp. 1–643, 1987.
- ²⁷Millhauser, G. L., E. E. Salpeter, and R. E. Oswald. Diffusion models of ion-channel gating and the origin of power-law distributions from single-channel recording. *Proc. Natl. Acad. Sci. USA* 85:1503–1507, 1988.

- ²⁸Sekizawa, S.-i., A. S. French, U. Höger, and P. H. Torkkeli. Voltage-activated potassium outward currents in two types of spider mechanoreceptor neurons. *J. Neurophysiol.* 81:2937–2944, 1999.
- ²⁹Sekizawa, S.-i., A. S. French, and P. H. Torkkeli. Low-voltage-activated calcium current does not regulate the firing behavior in paired mechanosensory neurons with different adaptation properties. *J. Neurophysiol.* 83:746–753, 2000.
- ³⁰Shannon, C. E., and W. Weaver. *The Mathematical Theory of Communication*. Urbana, Chicago and London: University of Illinois Press, pp. 1–117, 1949.
- ³¹Strout J., Conical: the computational neuroscience class library. *Proc. 18th Annu. Conf. Cogn. Sci. Soc.* 18:849, 1996.
- ³²Thorson, J., and M. Biederman-Thorson. Distributed relaxation processes in sensory adaptation. *Science* 183:161–172, 1974.
- ³³Toib, A., V. Lyakhov, and S. Marom. Interaction between duration of activity and time course of recovery from slow inactivation in mammalian brain Na⁺ channels. *J. Neurosci.* 18:1893–1903, 1998.
- ³⁴Torkkeli, P. H., and A. S. French. Simulation of different firing patterns in paired spider mechanoreceptor neurons: the role of Na⁺ channel inactivation. *J. Neurophysiol.* 87:1363–1368, 2002.
- ³⁵Torkkeli, P. H., S. Sekizawa, and A. S. French. Inactivation of voltage-activated Na⁺ currents contributes to different adaptation properties of paired mechanosensory neurons. *J. Neurophysiol.* 85:1595–1602, 2001.
- ³⁶Warland, D. D., M. A. Landolfa, J. P. Miller, and W. Bialek. Reading between the spikes in the cercal filiform hair receptors of the cricket. In: *Analysis and Modeling of Neural Systems*, edited by F. Eckman. Boston: Kluwer Academic, 1992, pp. 327–333.
- ³⁷Watts, R. E., and A. S. French. Sensory transduction in dorsal cutaneous mechanoreceptors of the frog, *Rana pipiens*. *J. Comp. Physiol. A* 157:657–665, 1985.